



## Modeling and application of direct contact membrane distillation for fluoride removal from aqueous solutions

Mekdimu Mezemir Damtie<sup>a</sup>, June-Seok Choi<sup>a,b,\*</sup>

<sup>a</sup>Department of Construction Environment Engineering, University of Science & Technology, (34113) 217, Gajeong-ro, Yuseong-gu, Daejeon, Korea, Tel. +82 10 5854 9475; email: mekdim@kict.re.kr

<sup>b</sup>Environment & Plant Engineering Research Institute, Korea Institute of Civil Engineering and Building Technology, (Daehwa-Dong) 283, Goyang-si, Gyeonggi-Do, 10223, Korea, Tel. +82 31 9100 759; Fax: +82 31 9100 291; email: jschoi@kict.re.kr

Received 29 January 2017; Accepted 13 November 2017

### ABSTRACT

The practicability of direct contact membrane distillation (DCMD) process for the removal of fluoride was investigated under different feed water, operational and membrane characteristics. Commercially available hydrophobic 0.22  $\mu\text{m}$  porous polytetrafluoroethylene (PTFE) and polyvinylidene fluoride (PVDF) membrane applied on fluoridated ultrapure water exhibit over 99% rejection of fluoride, yielding fluxes of up to 39.3 and 26.4  $\text{kg}/\text{m}^2\text{h}$  at 60°C, respectively. The dusty gas mathematical model and energy balance equations were employed to study the mass and heat transfer mechanisms. In addition to the good agreement between the theoretical and experimental comparison, the overall mass transfer analysis revealed that Knudsen–molecular–Poiseuille transition diffusion and Knudsen–Poiseuille diffusion are the dominant mass transfer mechanisms across the 0.22  $\mu\text{m}$  flat sheet PVDF and PTFE membranes, respectively. The effects of different parameters, such as temperature, initial fluoride concentration, feed flow rate, and membrane properties, on the flux and removal efficiencies were also evaluated, and feed temperature was found to be the most important operating parameter since higher temperatures induce the lowest temperature polarization coefficient (TPC) and a higher thermal efficiency (TE). Moreover, a wetting rate analysis in actual industrial wastewater sample indicated that a solution with higher organic matter, an membrane distillation (MD) system with PTFE membrane, and a sample with bigger initial fluoride concentration induce bigger wetting rate. Therefore, the DCMD process can be applied on fluoride affected water sources toward producing high-quality water suitable for a potable water supply. Exploiting renewable source potentials or industrial waste (free) energy will bring better economic advantage on the application.

*Keywords:* Fluoride removal; Direct contact membrane distillation; Mass transfer modeling; Wetting

### 1. Introduction

Fluoride in drinking water (mainly groundwater) emanates from natural rocks and some anthropogenic effects. Many countries in Australia, South Asia, South America, and North and East Africa have substantial amounts of fluoride in their water sources [1], and developing countries in

such areas are suffering from the health impacts of fluorosis. Fluoride at less than 1.5 mg/L [2] is required for our dental health, but fluoride amount between 1.5 and 4.0 mg/L causes dental fluorosis, and between 4.0 and 10 mg/L causes dental and skeletal fluorosis and greater than 10.0 mg/L causes paralysis, crippling fluorosis [3]. Moreover, long-term exposure to excess fluoride ion above the required limit also has additional complications such as failure on the foetus, low hemoglobin, inhibiting enzymes, distributed pain, and weakness

\* Corresponding author.

on joints, cancer, gastrointestinal problems, depression, urinary tract malfunctioning, sterility, malfunctioning of liver, kidney, and respiratory system [4,5]. Fluoride ingestion also has mental effects and brain cell damage [6].

Different physical and chemical defluoridation techniques, such as adsorption, coagulation, ion exchange, and membrane applications, have been introduced by scientists [7–10]. The application of membrane technology for fluoride removal is, however, tremendous and is one of the best practices as compared with the traditional physical and chemical techniques because a membrane process is an effective barrier to other physical, chemical, and biological pollutants as well [11]. Membrane process is a one-step process ensuring constant high-water quality, whereas the other conventional methods such as adsorption, coagulation, and ion exchange require more additional steps to complete the water treatment process [3,12]. Moreover, no or few chemicals are required in the membrane process as compared with the higher concentration of adsorbent and coagulant chemicals utilized in the adsorption and coagulation process [13]. The membrane process works under a wide pH range and yields nearly neutral pH filtrate, but other methods such as ion exchange method yield acidic water and the adsorption method works under narrow pH (5–6). In membrane process, interference of other ions is a not a problem as compared with the adsorption and ion exchange method in which some anions (e.g., sulfate, carbonate, etc.) significantly affects the performance. The problem of regeneration in membrane process is encountered less frequently as compared with frequent regeneration requirement in adsorption and difficult resin regeneration in the ion-exchange method [3]. However, the traditional methods are relatively cheaper as a cost of their poor removal efficiency.

The membrane process can be established in various ways based on the type of driving force and the feed water quality. Among these processes, MD is a membrane-based distillation process utilizing temperature difference to separate water vapor from feed water using hydrophobic porous membranes. The vapor pressure on either side of the membrane is induced by decreasing the temperature of the permeate side (condensing) and by increasing the temperature of the feed side water (evaporating) to a temperature that is lower than the boiling point of the feed water [14]. This lower temperature evaporation process on the feed side provides the benefit of utilizing low or waste heat energy for cheaper operation of the membrane distillation process. The mass transfer mechanism across the hydrophobic membrane is due to the vapor pressure difference, in which only water vapor can pass through the membrane and ultimately condense on the permeate side, while the hydrophobic nature of the membrane prevents liquid solutions from entering its pores due to surface tension forces [15,16]. Based on the arrangement of the permeate side of the membrane, four modular configurations have been found to be feasible in the MD process: the direct contact, air gap, sweeping gas, and vacuum type configurations. Among these modules, the DCMD technique is the simplest and most economical [17].

Currently, membrane distillation technology is receiving more attention from scientists as one of the best available next-generation desalination and water treatment technology. The most interesting attributes of this technology

include its less fouling tendency, complete solute rejection capability, and the use of relatively cheap and robust membranes. Moreover, this technology is a one-step treatment process using reduced pressure and waste energy to treat extremely polluted water [15–19]. However, MD is yet not at the level to be considered as a substitute for other membrane systems, though it can be considered for filling the gap of other existing systems, for instance through utilizing the system for RO brine treatment [20]. Despite increased attention on MD technology in the desalination discipline, less consideration has been given to its application for removal of fluoride and other inorganic contaminants, except that there are small and simple distillation apparatus demonstrated for household schemes [21]. The advancement of the MD technology, however, is now initiating various research work on fluoride removal using DCMD [12,22–24], but the novelty of this work lies in the fact that the effect of feed water composition (occurrence of organic and inorganic foulant), the MD membrane wetting analysis, and control methods have been addressed more in detail by using actual industrial wastewater. The application of DCMD on the removal of other inorganic pollutants, such as boron [25,26], arsenic [24,27,28], nitrate [29], chromium [30], and ammonia [31], has also been addressed recently.

The objective of this work is, therefore, to study the viability of the DCMD module (both from flux and removal efficiency point of view) as one of the alternative advanced treatment options for removal of fluoride ion from highly polluted industrial wastewater or groundwater sources. The specific objectives are to study how the theoretical model of the mass transfer mechanism across the membrane represents the experimental results and to investigate the wetting behavior and effect of membrane characteristics, operating conditions, and feedwater compositions on the fluoride removal from highly fluoridated industrial wastewater samples.

## 2. Theory

### 2.1. Theoretical and mathematical modeling of heat and mass transfer in DCMD

The heat and mass transfer mechanisms in the MD process are interrelated phenomena and should be dealt with simultaneously. Hence, a mathematical and schematic model for DCMD by considering simultaneous and balanced heat and mass transfer is described as follows.

#### 2.1.1. Mass transfer

Theoretically, the mass transfer mechanism through a porous membrane follows three steps: vaporization of the bulk, driving the vapor through the membrane using the difference in vapor pressure and ultimately condensing the vapor on the permeate side [17]. According to Darcy's law, this mass flux is assumed to have a linear relationship with the vapor pressure difference [32,33]:

$$J_w = B_m \Delta P_{ww} = B_m \times [P_{mf}^V - P_{mp}^V] \quad (1)$$

$$J_w = B_m \times [P_f^0 \times \gamma_{wf} \times \chi_{wf} - P_p^0] \quad (2)$$

where  $B_m$  is the membrane permeability coefficient ( $\text{kg m}^{-2} \text{s}^{-1} \text{Pa}^{-1}$ ),  $\Delta P_{\text{vw}}$  is the water vapor pressure difference (Pa),  $P_{\text{mi}}^V$  is the partial vapor pressure of the feed/permeate water (Pa),  $P_i^0$  is the pure water partial vapor pressure of the feed/permeate water (Pa),  $\gamma_{\text{wf}}$  is the water activity coefficient of the feed,  $\chi_{\text{wf}}$  is the mole fraction of water, and  $i$  represents either the feed or permeate side.

The mass transfer phenomena have been described in various ways by different scientists; however, the dusty gas approach has been widely employed in the study of membrane distillation [34–36]. Generally, there are four major trans-membrane mass transfer mechanisms: molecular diffusion, Knudsen diffusion, Poiseuille flow, and/or a combination of these. The membrane permeability coefficient and the dominant type of transport mechanism can be identified based on the Knudsen number,  $K_n$  [37,38].  $B_m^m$ ,  $B_m^k$ ,  $B_m^p$ , and  $B_m^c$  on Fig. 1 represent the mass transfer coefficients in molecular, Knudsen, Poiseuille, and combined flow regimes, respectively.

$$K_n = \frac{\lambda}{d_p} \quad (3)$$

$$\lambda = \frac{K_B \times T_m}{\pi \left( \frac{\delta_w + \delta_a}{2} \right)^2 \times P_a \times \sqrt{1 + \frac{M_w}{M_a}}} \quad (4)$$

where  $\lambda$  is the mean free path of transported molecules (m),  $K_B$  is the Boltzmann constant ( $1.38\text{E}-23$  J/K),  $P_a$  is the total pressure inside pores (Pa),  $T_m$  is the average membrane temperature (K),  $\delta_w$  is the collision diameter for water vapor (m),  $\delta_a$  is the collision diameter for air (m),  $M_w$  is the molecular weight of water (kg/mol),  $M_a$  is the molecular weight of air (kg/mol), and  $d_p$  is the pore diameter (m).

The estimated  $K_n$  value is often in the range of 0.11–0.55 since the pore size of MD membranes is 0.2–1.0  $\mu\text{m}$  and the mean free path of vapor is 0.11  $\mu\text{m}$ . Consequently, the combined Knudsen and molecular diffusion transport mechanism are commonly expected to dominate the mass transfer mechanism [39,40]. The Knudsen/molecular mechanism is expected to dominate when molecule–pore wall and molecule–molecule collisions occur in the microporous membrane [32]. However, the effect of Poiseuille flow neglected in most cases has also been considered here as a significant mass transfer component especially for bigger pore size membranes at higher temperature [41]. So it is worth considering the contribution of the Poiseuille flow in the MD mass transfer modeling and simulation works.

(a) Poiseuille flow

$$B_m^p = 0.125 \left( \frac{r^2 \varepsilon}{\tau \delta} \right) \left( \frac{M_w P_a}{\eta R T_m} \right) \quad (5)$$

(b)  $K_n < 0.01$  (molecular diffusion)

$$B_m^m = \frac{\varepsilon M_w P D_w}{\tau \delta R T_m P_a} \quad (6)$$

$$P D_w = 1.895 \times 10^{-5} \times T^{2.072} \quad (7)$$

(c)  $K_n > 1$  (Knudsen diffusion)

$$B_m^k = \frac{\varepsilon D_k}{\tau \delta R T_m P_a} \quad (8)$$

(d)  $0.01 < K_n < 1$  (transition mechanism: combined Knudsen–molecular–Poiseuille)

$$B_m^c = \left( \frac{1}{B_m^m} + \frac{1}{B_m^k} \right)^{-1} + B_m^p \quad (9)$$

$$B_m^c = \frac{\varepsilon M_w}{\tau \delta R T_m} \left[ \left( \frac{1}{D_k} + \frac{P_a}{P D_w} \right)^{-1} + 0.125 \left( \frac{P_a r^2}{\eta} \right) \right] \quad (10)$$

$$D_k = \frac{2}{3} r \sqrt{\frac{8 R T_m}{\pi M_w}} \quad (11)$$

$P D_w$  is water air diffusion ( $\text{Pa m}^2/\text{s}$ ) estimated from Eq. (7) [16], and  $\tau$ ,  $\delta$ ,  $\varepsilon$ ,  $r$ ,  $\eta$  are the membrane characteristics tortuosity, thickness (m), porosity, pore diameter (m), and viscosity of vapor air mixture (Pa s), respectively. Based on empirical models and a rule of thumb, the membrane tortuosity ( $\tau = 2$ ) is often recommended [16,42]. This value is not constant and often varies with temperature hence variation with temperature must be considered.

The vapor pressure difference between different sides of the membrane can be estimated from the membrane surface temperature using the most widely employed Antoine equation (Eq. (13)). However, the reduction in vapor pressure induced by the solute concentration should be considered using mole fraction and water activity coefficients. Accordingly, the vapor pressure for aqueous salt solutions at the membrane surface can be estimated as follows [43,44]:

$$P_{\text{mf}}^V(T_{\text{mf}}, \chi_{\text{wf}}) = P_f^0(T_{\text{mf}}) \gamma_{\text{wf}}(T_{\text{mf}}, \chi_{\text{wf}}) \quad (12)$$

where  $\gamma_{\text{wf}}(T_{\text{mf}}, \chi_{\text{wf}})$  is the water activity of the solution,  $\chi_{\text{wf}}$  is the mole fraction of water =  $1 - \chi_s$ ,  $\chi_s$  is the mole fraction/percent of solute,  $T_{\text{mf}}$  is the temperature of the feed, and  $P_f^0(T_{\text{mf}})$  is the vapor pressure of pure water as estimated by the Antoine equation [45]:

$$P_i^0 = \exp \left( 23.1964 - \frac{3816.44}{T_{\text{mi}} - 46.13} \right) \quad (13)$$

### 2.1.2. Heat transfer

The heat transfer through the entire DCMD process is achieved in three different components and media (Fig. 1). First, the heat transfer is achieved because of a hot side temperature polarization in the bulk feed solution. Then, second, the heat transfer in the membrane body can be achieved simultaneously in two ways: due to conductive heat transfer of the membrane material, and heat transfer through the vapor diffusion. And third, heat transfer can be achieved due to cold temperature polarization in the cold side [40,46]. Fig. 1 shows the heat transfer model equations and schematics of

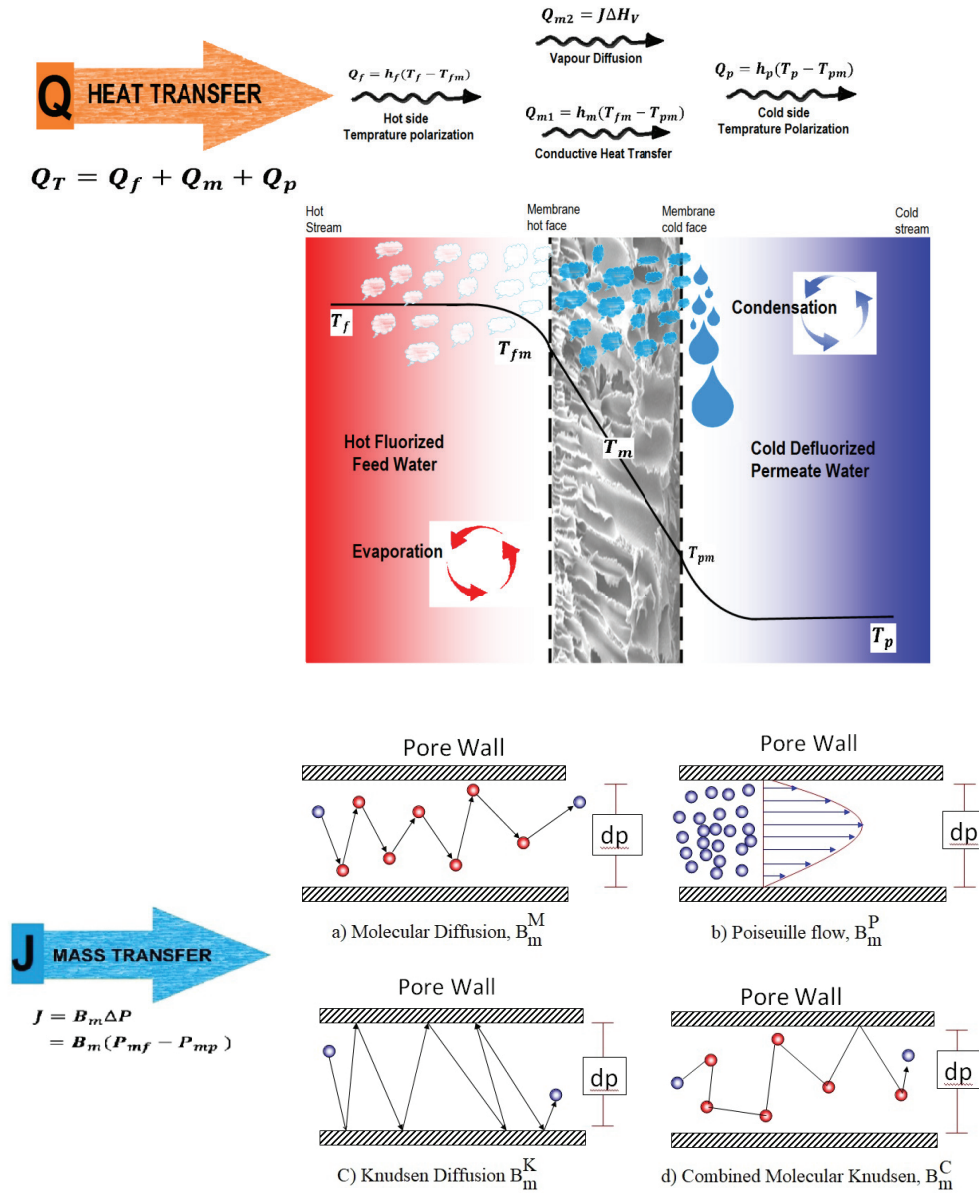


Fig. 1. Schematic representation of heat transfer components, mass transfer mechanisms, and DCMD treatment process.

heat transfer components. Among all these four components, the heat transfer induced by mass diffusion in the membrane body is significant. However, the heat transfer amount on the feed and permeate boundary layer is almost negligible [33].

From the assumption of steady-state conditions, the overall heat balance equations can provide a better estimation of the membrane surface temperature on both sides:

$$Q_{\text{feed}} = Q_{\text{membrane}} = Q_{\text{permeate}} \quad (14)$$

$$T_{\text{mf}} = \frac{\frac{K_m}{\delta} \left( T_p + \left( \frac{h_f}{h_p} \right) \times T_f \right) + h_f \times T_f - J_w \Delta H_v}{\frac{K_m}{\delta} + h_f + \frac{K_m}{\delta} \times \frac{h_f}{h_p}} \quad (15)$$

$$T_{\text{mp}} = \frac{\frac{K_m}{\delta} \left( T_f + \left( \frac{h_p}{h_f} \right) \times T_p \right) + h_p \times T_p + J_w \Delta H_v}{\frac{K_m}{\delta} + h_p + \frac{K_m}{\delta} \times \frac{h_p}{h_f}} \quad (16)$$

$$K_m = \left[ \frac{\varepsilon}{K_g} + \frac{(1-\varepsilon)}{K_p} \right] \quad (17)$$

where  $h_f$ ,  $h_m$ , and  $h_p$  are heat transfer coefficients in the feed, membrane, and permeate, respectively ( $\text{W}/\text{m}^2 \text{K}$ ), and  $K_m$  is the effective thermal conductivity of a porous membrane ( $\text{W}/\text{m K}$ ), which can be estimated from the isostress model using the thermal conductivity of vapor ( $K_g$ ) and membrane polymer material ( $K_p$ ) [16,36]:

$$h_i = \frac{Nu_i \times K_{wi}}{D_h} \quad i = f \text{ or } p, \quad (18)$$

where  $i$  stands for the feed or permeate,  $D_h$  is the hydraulic diameter,  $Nu$  is the Nusselt number estimated based on the Reynolds number (Re) and Prandtl number (Pr).

$$Re = \frac{\rho v D_h}{\mu} \quad (19)$$

$$Pr = \frac{C_p \mu}{K_m} \quad (20)$$

where  $\rho$ ,  $\mu$ ,  $v$ , and  $C_p$  are the density of water ( $\text{kg/m}^3$ ), dynamic viscosity ( $\text{kg/m s}$ ), average velocity ( $\text{m/s}$ ), and specific heat ( $\text{J/kg K}$ ) of the fluid, respectively. Care should be taken because the magnitude of this fluid and air vapor properties vary significantly with temperature; hence their values have to be measured or calculated by taking the feed side temperature variation into consideration.

The hydraulic diameter,  $D_h$ , will be estimated from the geometry of the flow channel using:

$$D_h = \frac{\text{Cross-sectional area}}{\text{Wetted perimeter}} = \frac{4 \times A_c}{P_w} \quad (21)$$

where  $A_c$  is the cross-sectional area of the flow channel at a different position ( $\text{m}^2$ ) and  $P_w$  is the wetted perimeter ( $\text{m}$ ).

Various experiments and studies have been suggested by researchers for estimating the value of the Nusselt number from different flow and module parameters. However, there are significant discrepancies among the values predicted by different empirical equations, so it is often difficult to decide which model is the best. Therefore, most commonly suggested Nusselt number estimation is selected from different studies [18,32,36,47]. Eq. (22) is employed for the laminar flow system ( $Re < 2,100$ ) and Eq. (23) for the turbulent flow system ( $Re > 2,100$ ). The Reynolds number estimation in this experiment shows that the flow is in both laminar and turbulent regime:

$$Nu = 0.097 \times Re^{0.73} Pr^{0.13} \quad (22)$$

$$Nu = 0.023 \times Re^{0.8} Pr^{1/3} \quad (23)$$

For ease of programming and for understanding the entire procedure and predicting iterative optimal flux from different input parameters (module property, operational, physical and membrane characteristic), a flow chart has been constructed, as shown in Fig. 2.

### 2.1.3. Thermal analysis

Because membrane distillation technology is a thermally driven system, dealing with and understanding the entire thermal process is essential. This thermal study mainly addresses the heat transfer mechanism across the feed boundary layer limiting the mass transfer, because the thermal boundary layer resistance near the membrane surface

plays an important role in the heat transfer mechanism [32]. This boundary layer process can be studied via the TPC and TE, which can be estimated using the following equations:

$$TPC = \frac{T_{fm} - T_{pm}}{T_f - T_p} \quad (24)$$

$$TE = \frac{J \Delta H_v}{J \Delta H_v + \left( \frac{K_m}{\delta} \right) \times (T_{fm} - T_{pm})} \times 100\% \quad (25)$$

### 2.2. Factors affecting performance of DCMD process

The fluoride rejection in all these experiments under several conditions by both PVDF and PTFE hydrophobic membranes is large enough to warrant sufficient rejection of the fluoride ion. However, the economic and optimal utilization of the process entails a deep understanding of the major factors affecting permeability and overall rejection performance of the module. The DCMD process is mainly affected by three major categories of adjustable parameters [48,49]. These are the membrane parameters (pore size, membrane material, thickness, porosity, hydrophobicity, etc.), the operational parameters (temperature, flow rate, initial fluoride concentration, etc.) and the feed water composition parameters (existence of organic and inorganic matters). In the following sections, all these factors affecting the rejection and permeate yield will be discussed with more detailed attention on the effect of feed water composition with its possible reversibility mechanisms.

Despite the various advantages of the MD technology over other advanced systems, the fouling phenomenon is now emerging as a major concern. The MD process can be controlled and operated well if there is no fouling that causes wetting [50]. Among the main fouling categories of MD, organic fouling accounts for fouling that occurs due to natural organic matter (e.g., humic/fulvic substances). Humic matter in the feed water reduces the flux and causes surface wetting because of the formation of a thick gel layer of a macromolecular substance on the membrane surface and a reduction in the electrostatic repulsion between humic acid molecules. This behavior mainly emanates from amphipathic and negatively charged nature of humic acids that result from the dissociation of carboxylic acid and hydroxyl functional groups. Organic fouling also reduces membrane hydrophobicity and increases total organic carbon in the permeate [14,20,50,51].

A substantial number of experiments have been conducted to study the significant effect of humic acid on MD performance and efficiency, especially with the existence of salt ions. In this study, however, the effect on the flux, wetting rate, and removal efficiency will be addressed in an aqueous solution without any salt. As per a recent study [14], mass-transfer coefficients of water vapor through the PTFE and PVDF membranes in a humic acid solution is nearly identical, except for the minor flux difference, which originates mainly from their differences in temperature polarization and heat transfer resistance tendencies. Hence, only the hydrophobic PTFE membrane was employed here to study the effect of organic and inorganic fouling.

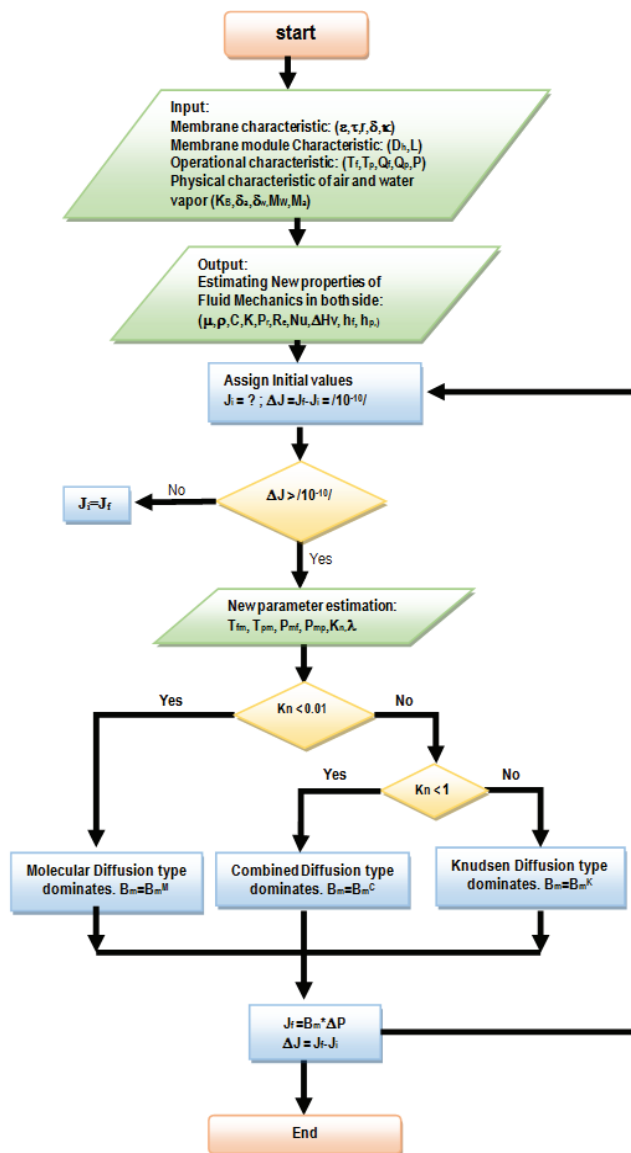


Fig. 2. Iterative model flow chart to calculate optimal mass flux.

### 3. Materials and methods

#### 3.1. Membrane and membrane module

Commercially available hydrophobic porous PVDF and PTFE membranes were used in the laboratory at the bench scale. The module type utilized for this experiment is a DCMD module with an effective area of 0.0043 m<sup>2</sup>, a channel depth of 1 mm, and a feed volume of 1 L. The experiment was conducted at various velocities (0.5–2 L/min), fluoride concentrations (2–6,000 mg/L), and feed temperature scenarios (20°C–70°C). Table 1 shows the key characteristics of the membranes and module used as specified by manufacturers and analyzed in the laboratory.

#### 3.2. Experimental setup

The schematics of the experimental setup of the entire DCMD module are shown in Fig. 3. The system operates

in such a way that, first the fluoridated hot solution was circulated through the feed side of the membrane module, while cold deionized water was also circulated on the permeate side of the membrane module. This simultaneous operation of both sides of the membrane tends to move the water vapor from the feed side to the permeate side via the hydrophobic membrane. The water circulation over the membrane surface is conducted by pumping both the hot feed and cold permeate water to their reservoirs via a variable speed pump (Cole-Parmer Instrument, company Model 75211-15, USA). Similar types of the pump have been utilized for both feed and permeate side. The feed solution is then evaporated by a heater (Lab Companion BW10H heating bath) and the produced water on the permeate side is condensed by a chiller (CPT Inc. (Korea) refrigerated bath circulator). This process is then repeated with different temperatures, flow rates, and concentration values. The required flow rate is accurately adjusted on both pumps before the experiment and has been checked several times. The feed side and permeate side temperatures are then adjusted on the chiller and cooler and continuously measured by an automatic temperature and EC measuring device (WTW-Multi 3410). The treated permeate mass flux data are captured via a control PC, which is wired to a OHAUS Explorer Pro Electronic digital balance, and data are recorded at every stage (minute) throughout the duration of the experiment. The liquid entry pressure (LEP) for all membrane types (Table 1) is measured using a small digital pressure sensor (10.00 bar, Autonics PSA-1) and the contact angle using a SV Sigma 701 Tensiometer from KSV Instruments Ltd. (Helsinki, Finland).

#### 3.3. Fluoride removal experiment and wetting analysis

To study the DCMD modeling and compare with actual experimental results, a synthetic fluoridated feed solution was prepared using solid sodium fluoride (purchased from Showa, Japan) and ultrapure deionized water processed under a multi-stage water purification process (Puris RO water system). Different concentrations of fluoridated samples were prepared by diluting the stock solution with deionized water. The fluoride concentration in any feed or permeate water sample was measured using a Dionex ICS-3000 Ion Chromatography System (Metrohm AG, Switzerland) and the alkalinity of the feed solution was controlled by a pH meter (Thermo Scientific, Singapore, Orion Star series pH meter). However, to study the wetting phenomenon induced by different type of feed water composition, highly polluted synthetic industrial wastewater samples (Table 2) that can better represent the wastewater samples from fluoride releasing industry have been prepared in the laboratory from commercially available different compounds. These compounds are NaF and NaOH (Showa, Japan), CaCl<sub>2</sub> (Kanto Chemical, Japan), MgCO<sub>3</sub> (Katayama Chemical Industries, Japan), KNO<sub>3</sub>, HCl, KH<sub>2</sub>PO<sub>4</sub> (Samchun Pure Chemical, Korea), humic acid (Sigma-Aldrich, Switzerland), MnSO<sub>4</sub>·H<sub>2</sub>O (Paejung chem., Korea). SEM and EDX have been analyzed using high resolution field emission scanning electron microscopy (FESEM) S-4300 SE SEM and EDX (Hitachi, Tokyo, Japan) with Q150T Turbo-Pumped sputter platinum coater (Quorum Technologies Ltd., UK).

Table 1  
Membrane and module characteristics used for the experiment

Membrane type	PVDF	PTFE
Manufacturer source	Millipore	Millipore
Model	Durapore/GVHP14250	Fluoropore/FGLP29325
Average pore size ( $\mu\text{m}$ )	0.22/0.45	0.22
Liquid entry pressure (bar)	2.30	4.85
Porosity (%)	0.75	0.78
Effective membrane length (m)	0.095	0.095
Effective membrane area ( $\text{m}^2$ )	0.0043	0.0043
Thickness (m)	0.000125	0.000085
Thermal conductivity (W/m K)	0.043	0.092
Pore tortuosity	2.0	2.0
Contact angle	$127.3^\circ \pm 2.6^\circ$	$143^\circ \pm 3.2^\circ$
RMS membrane roughness (nm)	39	71
Module type and characteristic		
Type of module:	Direct contact membrane distillation	
Material type	High density polyethylene (HDPE)	
Size of the module	95 mm $\times$ 46 mm	
Effective membrane area ( $\text{m}^2$ )	0.0043	
Channel depth	1 mm	
Feed volume size	1 L	
Flow channel hydraulic diameter	4 mm	
Feed side tube length	6.6 m	
Permeate side tube length	5.6 m	
Permeate side fixed temperature	20°C (273 K)	

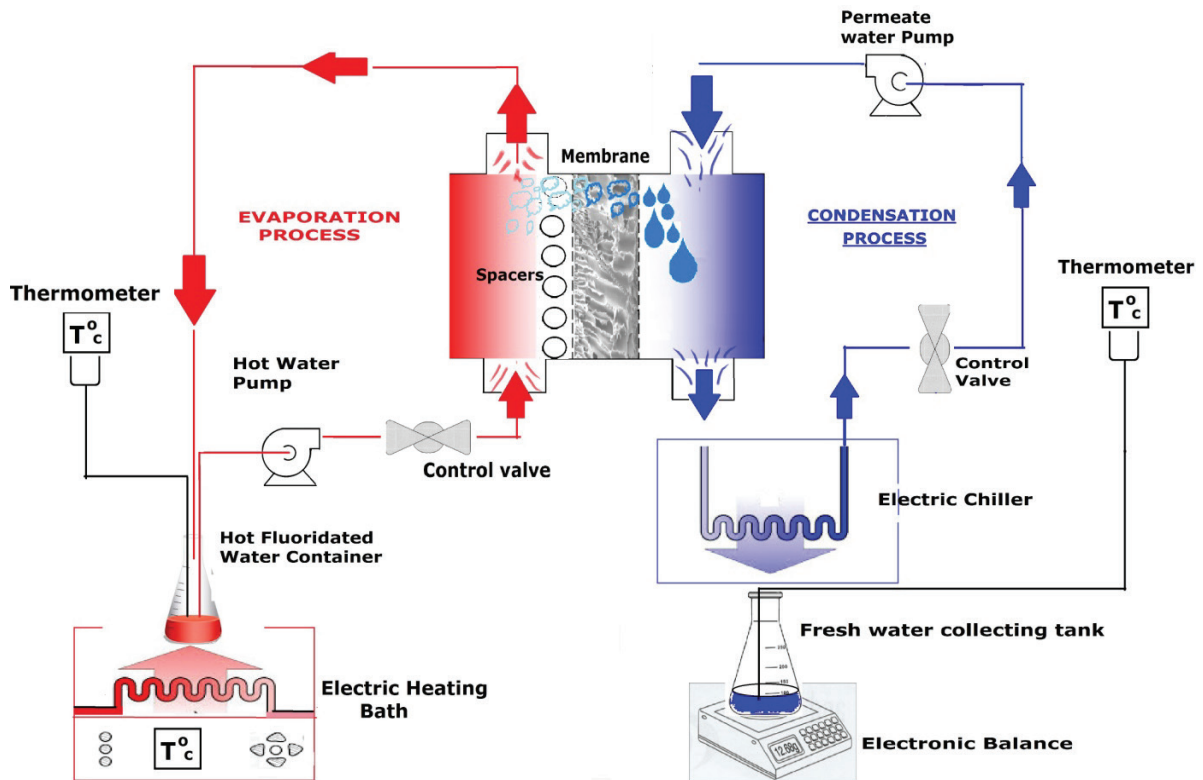


Fig. 3. Schematics of the direct contact membrane distillation unit.

Table 2  
Model vs. experimental result comparison for PVDF 0.22  $\mu\text{m}$  membrane

Feed temperature (K)	Estimated vapor pressure (Kpa)	Measured and experimental permeate flux (kg/m <sup>2</sup> h)		Model error	
		Experimental value	Model output (KMP)	Root mean-square error (RMSE)	Mean absolute percentage error (MAPE)
303	4.63	2.70	2.48	0.05	0.082
313	8.07	6.90	6.44	0.22	0.067
323	13.51	13.59	12.36	1.51	0.091
333	21.83	21.83	20.76	1.15	0.049
343	34.16	31.72	32.06	0.12	0.011
				<b>0.78</b>	<b>6%</b>

Values in bold are the actual overall values of RMSE and MAPE. Condition: Permeate and feed volumetric flow rate = 1 L/min, fluoride concentration = 20 mg/L, permeate side temperature = 20°C.

### 3.4. Mass flux

The average permeate mass flux ( $J_w$ ) was measured from the overflow volume of the permeate reservoir on the electronic balance and calculated as follows:

$$J_w = \frac{\Delta m}{A_m \times t} \quad (26)$$

where  $\Delta m$  is the mass flux recorded per unit time (kg),  $A_m$  is the effective utilized area of the membrane ( $86 \times 36 \text{ mm} = 0.00036 \text{ m}^2$ ), and  $t$  is the time interval at which the mass flux of the permeate is recorded (min) and changed to hour (h) later.

### 3.5. Fluoride rejection efficiency

The fluoride removal efficiency (%) can be calculated by measuring the initial feed concentration of the hot feed side and the final permeate side:

$$\text{Removal efficiency} = \frac{C_f - C_p}{C_f} \times 100\% \quad (27)$$

where  $C_f$  is the feed side concentration and  $C_p$  is the permeate side concentration.

### 3.6. Saturation index calculation

The fluoride precipitation rate and speciation has been predicted using Visual MINTEQ 3.1 chemical equilibrium model (Jon Petter Gustafsson, KTH, Sweden, 2000) by calculating the saturation index value (SI) with the following general equation:

$$\text{SI} = \log_{10} \frac{\text{IAP}}{K_{\text{SP}}} \quad (28)$$

where IAP is the ion activity product and  $K_{\text{SP}}$  is the solubility product constant.

## 4. Results and discussion

### 4.1. Experimental and theoretical model comparison

To evaluate the prediction competency of models discussed previously, the experimental mass flux permeates data

collected in the laboratory were compared with the model outputs. A simple spreadsheet and MATLAB code were utilized to estimate the theoretical mass flux. All possible mass transport mechanisms in the membrane (Knudsen, molecular, and Poiseuille) and their possible combination have been considered for the analysis. Accordingly, the result obtained using PVDF membrane, indicated in Fig. 4, shows that among these models, both the molecular (M) and Knudsen (K) diffusion models are overestimating and Poiseuille flow (P) model is underestimating the experimental results, and they show significant variation from the experimental result. On the other hand, the combination of the Poiseuille flow, Knudsen, and molecular diffusion models (KMP), indicated in Table 2, shows good agreement with the experimental results. In addition, the mean free path of the water vapor at different temperatures in this experiment varies from 0.107 to 0.115  $\mu\text{m}$ , which is significantly less than the 0.22  $\mu\text{m}$  average pore size of the PVDF membrane utilized for the experiment. Subsequently, the estimated Knudsen numbers for different feed temperatures (0.47 to 0.51) fall in the range of  $0.01 < K_n < 1$ . Therefore, all these model parameters and graphical compliance indicate that the transport of water vapor molecule follows all the three kinds of transport phenomenon through the membrane pores, and the combined Knudsen–molecular–Poiseuille is the dominant mass transfer mechanism in 0.22  $\mu\text{m}$  PVDF membrane. There are previous works that reported identical result [41].

Likewise, for the PTFE membrane, the result shown in Fig. 5 and Table 3 indicates that the experimental data collected under the same conditions fit with the Knudsen–Poiseuille (KP) mass diffusion mechanism. Moreover, the estimated mean free path value is nearly equivalent to the pore diameter of the membrane and the Knudsen number,  $K_n$  is between 0.97 and 1.05. These clearly signify the dominance of the Knudsen type diffusion in the entire water vapor transport through the PTFE membrane. This result also agrees with some other previous works [30,52,53].

In general, the  $K_n$  value and the comparison of experimental vs. estimated flux reveal that the mass transport in the PVDF membrane has more of the dominance of the molecular diffusion and that of the PTFE membrane has the dominance of the Knudsen diffusion. These are the reasons why the PTFE membrane has much higher permeate flux than that of PVDF (refer the experimental result on Fig. 6), as membranes

having a lot of pore sizes in the Knudsen region have higher flux. On the other hand, those membranes having a lot of pore sizes in the molecular diffusion regime (e.g., the PVDF membrane in our case) will have a better rejection efficiency even though their permeate flux is relatively smaller. Refer

Section 4.3 to see the relative comparison of the rejection efficiency of the PVDF and PTFE membranes.

The significant difference in the mass transfer mechanism and magnitude among these two membranes is attributable mainly to their physical characteristics and their interaction with the water vapor molecule. These include less mass transport resistance, higher TE, and better heat transfer tendency of the PTFE membrane (Figs. 8 and 9) attained as a result of different membrane material type use and fabrication methods. The most prevalent relative membrane characteristics (Table 1) worth mentioning about the higher flux of PTFE over PVDF membrane include: thickness, porosity, membrane roughness, and hydrophobicity (contact angle and LEP). The PTFE membrane utilized in this experiment has relatively a smaller membrane thickness which significantly affected the thermodynamic effects of the system, and in turn, could increase the flux. This is because thicker membrane structures impose retarded movement and higher mass transfer resistance of vapor diffusion inside the membrane pore which subsequently favors build-up of boundary layer thickness on the membrane interface. This boundary layer eventually reduces the flux. From the general equation of permeate yield (Eqs. (5), (6), (8), and (10)), we can also observe that permeability is a function of reciprocal of membrane thickness [45]. The effect of this membrane

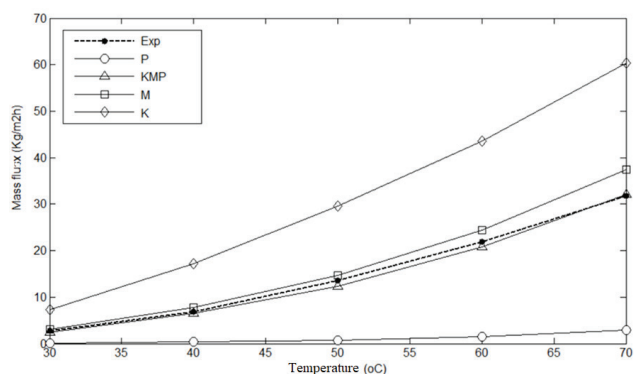


Fig. 4. Experimental vs. estimated permeate flux as a function of feed temperature for 0.22  $\mu\text{m}$  PVDF membrane (permeate temperature = 20°C; feed/permeate flow rate = 1 L/min/1 L/min; fluoride concentration = 20 mg/L).

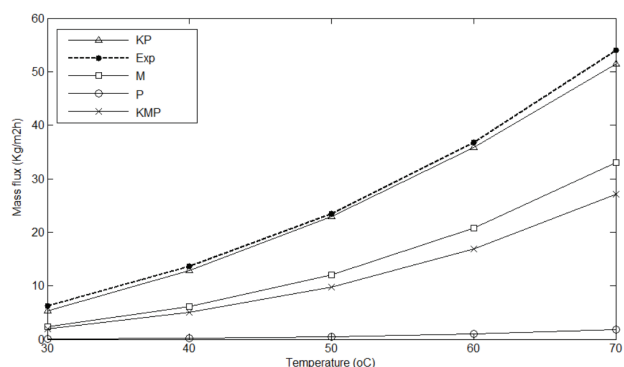


Fig. 5. Experimental vs. estimated permeate flux as a function of feed temperature for 0.22  $\mu\text{m}$  PTFE membrane (permeate temperature = 20°C; feed/permeate flow rate = 1 L/min/1 L/min; fluoride concentration = 20 mg/L).

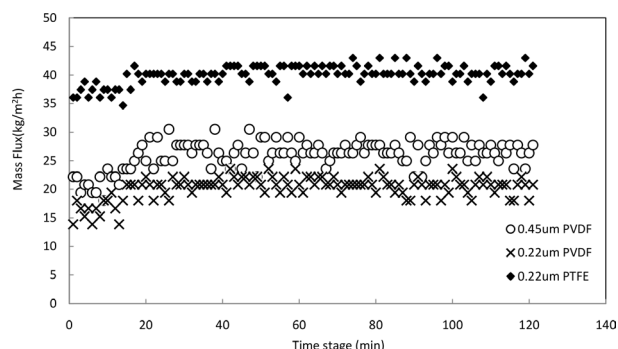


Fig. 6. Permeate flux vs. time comparison of membranes with different material and pore size (feed/permeate temperature: 60°C/20°C; feed/permeate flow rate = 1 L/min/1 L/min; fluoride concentration = 20 mg/L).

Table 3  
Model vs. experimental result comparison for PTFE 0.22  $\mu\text{m}$  membrane

Feed temperature (K)	Estimated vapor pressure (Kpa)	Measured and experimental permeate flux (kg/m <sup>2</sup> h)		Model error	
		Experimental value	Model output (KP)	Root mean-square error (RMSE)	Mean absolute percentage error (MAPE)
303	4.63	6.24	5.29	0.92	0.15
313	8.07	13.59	12.84	0.57	0.06
323	13.51	23.50	23.00	0.25	0.02
333	21.83	36.75	35.91	0.70	0.02
343	34.16	54.00	51.52	6.15	0.05
				1.31	5.98%

Condition: Permeate and feed volumetric flow rate = 1 L/min, fluoride concentration = 20 mg/L, permeate side temperature = 20°C.

thickness will be more significant at a higher temperature. Second, the higher porosity in PTFE membrane can also be one of the reasons for higher permeate flux, as increasing the porosity increases the surface area available for water vapor transport and lower the conductive heat loss [18]. Moreover, the higher surface roughness of the PTFE membrane (even more on the support layer side) abet mixing at the membrane interfaces toward improving the hydrodynamic condition and reduce the boundary layer thickness which positively affects the permeate flux. The roughness also significantly reduces the wettability of the membrane and provides more sustained permeate production [24,29]. Finally, the higher contact angle and LEP of the PTFE membrane utilized for this experiment also confirms relatively a better hydrophobicity than the PVDF membrane. This hydrophobicity is a major characteristic of MD membranes that greatly affects the vapor transport rate. In membranes with higher hydrophobicity, there is a higher tendency for the vapor to easily pass through the membrane pores, so that higher distillate flux can be obtained. As long as the applied pressure is within LEP limit, feed liquid cannot penetrate through the MD pores [18,54].

#### 4.2. Effect of different operating parameters

##### 4.2.1. Temperature and vapor pressure

The effect of temperature on the mass flux and fluoride rejection efficiency is evaluated in the range of 20°C–70°C under various volumetric flow rates using the PTFE membrane (refer to Fig. 7 and Table 4). Accordingly, increasing the feed side temperature results in a higher mass flux magnitude, because a temperature increase tends to increase the driving vapor pressure force in an exponential trend, as explained by the Antoine's equation (Eq. (13)). This indicates that the mass flux, vapor pressure, and feed temperature are strongly correlated parameters. In addition, a temperature increase also decreases the thickness of the boundary layer and the viscosity of the fluoridated feed water so that the mass transfer will be enhanced. Consequently, for better flux, maximum TE and higher polarization are advisable to operate the MD system at a higher feed temperature. On the other hand, except dilution effect, there is no evidence that temperature directly affects the fluoride rejection

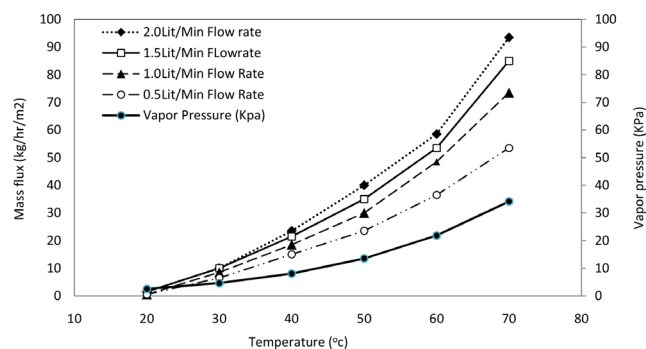


Fig. 7. Permeate mass flux and vapor pressure vs. temperature (permeate side temperature = 20°C; permeate volumetric flow rate = 1 L/min, fluoride concentration = 20 mg/L, PTFE membrane).

efficiency, because the permeate fluoride concentration persistently remains less than 0.55 mg/L. Rejection efficiency above 99.87% has been achieved under all feed temperature conditions. This agrees with some other relevant previous studies [22,25].

In addition to the feed temperature effect, two more systematic parameters, TPC and TE (Eqs. (24) and (25)), have been utilized to undertake the thermal analysis of the system for both the PTFE and PVDF membranes (Figs. 8 and 9, respectively). Accordingly, increasing the feed temperature from 20°C to 70°C decreases the temperature polarization from 0.73 to 0.30 in PTFE and from 0.83 to 0.61 in PVDF, which clearly shows that TPC of PTFE is lower than that of PVDF membrane. This is because the thermal conductivity of PVDF membrane (Table 1) is significantly less than that of PTFE membrane subsequently there will be lower heat losses in PVDF than PTFE. However, regardless of the lower thermal conductivity in PVDF membrane, increasing the feed temperature resulted in an increase in the TE of PTFE from 78% to 97% and that of PVDF from 55% to 90%. This relatively better TE increase in PTFE at a higher temperature generally asserts the superior utilization of heat energy for vaporization than for conduction heat loss via the membrane. At higher temperature, the effect of heat loss through conduction will be highly suppressed, so that most of the heat transfer to the permeate side will be performed through the mass transfer, not through conduction.

Table 4

Ionic constituents and composition of different wastewater samples

Ionic compositions	Sample 1: Inorganic matter with high fluoride Sample 2: Organic matter with high fluoride Sample 3: Both inorganic and organic matter with high fluoride Concentrations (mg/L)		
	Sample 1	Sample 2	Sample 3
<b>Cations:</b>			
Ca <sup>+2</sup>	252		252
Mg <sup>+2</sup>	194.6		194.6
Fe <sup>+2</sup>	20		20
K <sup>+1</sup>	25.3		25.3
Na <sup>+1</sup>	605	1,326	605
Al <sup>+3</sup>	23		23
Mn <sup>+2</sup>	8		8
<b>Anions:</b>			
F <sup>-</sup>	1,100	1,100	1,100
Cl <sup>-</sup>	565.2		565.2
SO <sub>4</sub> <sup>-2</sup>	729.7		729.7
NO <sub>3</sub> <sup>-</sup>	31		31
CO <sub>3</sub> <sup>-2</sup>	110		110
PO <sub>4</sub> <sup>-2</sup>	14.6		14.6
<b>Others</b>			
SiO <sub>2</sub>	1,500		1,500
Humic acid		30	30

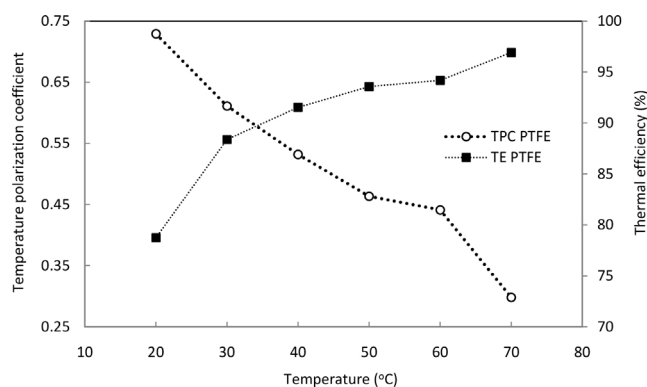


Fig. 8. Temperature vs. temperature polarization coefficient and thermal efficiency of PTFE membrane (permeate side temperature = 20°C; feed and permeate volumetric flow rate = 1 L/min; fluoride concentration = 20 mg/L).

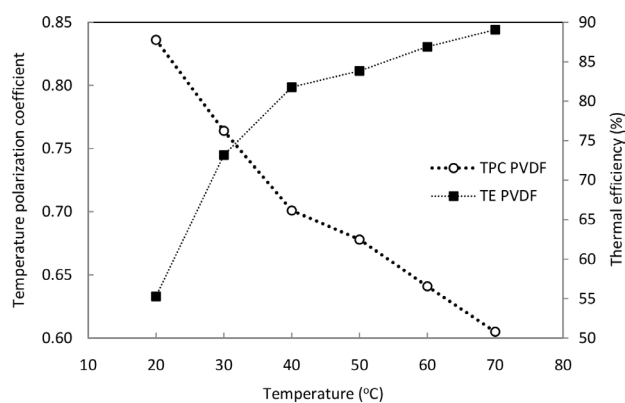


Fig. 9. Temperature vs. temperature polarization coefficient and thermal efficiency of PVDF membrane (permeate side temperature = 20°C; feed and permeate volumetric flow rate = 1 L/min; fluoride concentration = 20 mg/L).

#### 4.2.2. Volumetric flow rate

An experiment was undertaken to study the effect of different flow velocities (ranging from 0.5 to 2 L/min under a temperature range from 20°C to 70°C) on the permeate flux and fluoride removal efficiency. Figs. 7 and 10 show the variation in the permeate flux as a function of different flow rates. The effect of flow rate on the mass flux mainly depends on the temperature because the permeate flux is almost constant at lower temperatures and tends to increase at higher temperatures. Hence, the flow rate does not significantly affect the flux at lower temperatures, but at higher temperatures, the flux tends to increase a little bit up to certain critical flow rate values and then stay asymptotically to the constant flux. This is because enhanced heat conduction across the membrane decreases the vapor driving force. The increase in the flux due to high flow rate, at higher temperatures is attributable to the improvement of the hydrodynamic condition at the membrane surface due to the enhancement of the Reynolds number as the flow rate increases. When the Reynolds number increases, it increases the turbulence and decreases the temperature polarization and boundary layer thickness, which in turn appreciably affects the driving force and mass transfer coefficient [54].

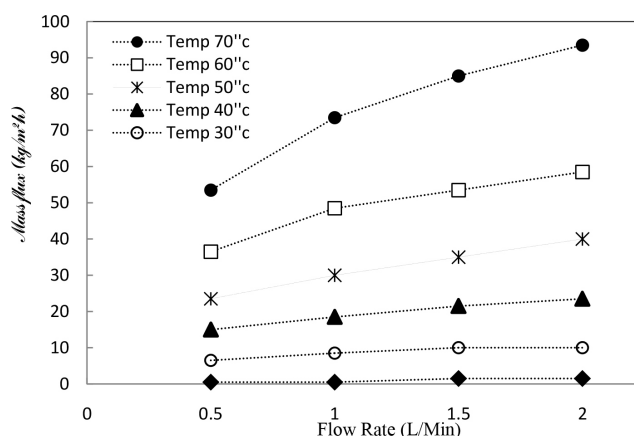


Fig. 10. Mass flux vs. volumetric flow rate at different feed temperature (permeate side temperature = 20°C; permeate volumetric flow rate = 1 L/min; fluoride concentration = 20 mg/L; membrane type = PTFE).

On the other hand, the effect of flow rate on the rejection efficiency is found to be negligible, because varying the flow rate from 0.5 to 2.0 L/min reduced the efficiency from 99.93% to 99.90%. This slight reduction of the fluoride rejection efficiency might be an error in the accuracy of the measuring device because measuring fluoride at such very small concentrations is full of uncertainty. However, at higher flow rates, there might still be a possibility that a reduction in efficiency might occur because of the escape of some fluoride ions either through the partially wetted membrane areas (induced from the hydraulic force) or through some bigger pores that result from a non-uniform pore size distribution (induced from manufacturing defect).

#### 4.3. Wetting analysis and control methods using actual wastewater

Industrial wastewater from steel, semiconductor, fertilizer, and glass manufacturing industry is the most common wastewater samples likely to have copious fluoride ion concentrations reaching up to 3,000 mg/L [55,56]. Three major factors; initial fluoride concentration, membrane material type, and the feed water composition, have been selected to study the wetting rate of fluoride ion through the DCMD system.

##### 4.3.1. Effect of initial fluoride concentration

The influence of the initial fluoride feed concentration on the permeate flux and rejection efficiency has been studied in two major ways. First using a pure feed water solution with a fluoride concentration ranging from 2 to 1,000 mg/L and second using an actual wastewater (sample 3 of Table 4) with higher initial fluoride concentration ranging from 1,000 to 6,000 mg/L. Consequently, in the first experimental result (Figs. 11 and 12) varying the initial fluoride concentration does not have any detectable effect on the mass flux. This value was checked both experimentally and theoretically using the combined Knudsen–molecular–Poiseuille diffusion model (for PVDF) and Knudsen–Poiseuille model (for PTFE) in that both the measured and calculated mass flux values

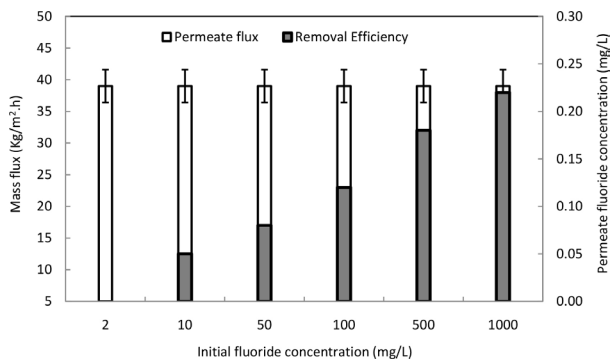


Fig. 11. Flux and removal efficiency vs. initial fluoride ion concentration (feed side/permeate side temperature = 60°C/20°C; feed/permeate volumetric flow rate = 1 L/min/1 L/min; membrane type = PTFE).

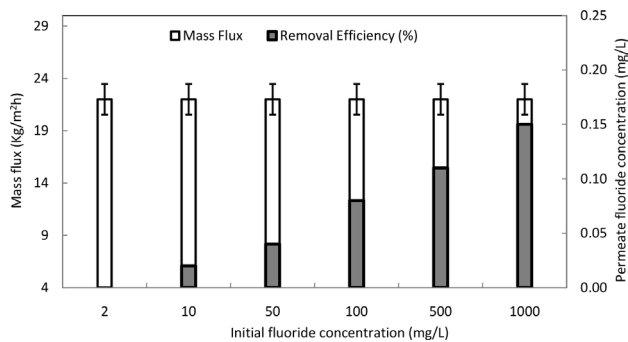


Fig. 12. Flux and removal efficiency vs. initial fluoride ion concentration (feed side/permeate side temperature = 60°C/20°C; feed/permeate volumetric flow rate = 1 L/min/1 L/min; membrane type = PVDF).

hold the usual swinging values in between  $\pm 6.64\%$  from 25 kg/m<sup>2</sup> h for PVDF and  $\pm 5.21\%$  from 38 kg/m<sup>2</sup> h for PTFE. A similar result has been reported previously [22,23]. On the other hand, the effect of increasing the initial fluoride concentration also exhibits small influence on the removal efficiency. Figs. 11 and 12 show that 0.22 mg/L and 0.15 mg/L of fluoride has been detected for 1,000 mg/L of initial fluoride concentration for PTFE and PVDF, respectively, which is actually below the World Health Organization (WHO) drinking standard of 1.5 mg/L. This small loss in efficiency is attributable to the escape of some fluoride ions through partial wetting or through a few large pores in the non-uniform pore size distribution membrane.

In the same manner, an experiment using an actual wastewater (sample 3) and very high concentration of fluoride ion (1,000–6,000 mg/L) revealed that increasing the initial fluoride concentration in the feed solution from 1,000 to 3,000 mg/L then to 6,000 mg/L significantly decreased the initial permeate flux from 42 to 36 kg/m<sup>2</sup> h and to 31.2 kg/m<sup>2</sup> h (Fig. 13). This is because an increase in the feed concentration increases the viscosity and concentration polarization effect in the boundary layer and then ultimately suppresses the mass transfer coefficient. Moreover, it can also be observed that increasing the initial fluoride ion concentration exhibits substantial increment in the wetting rate. As can be referred in Fig. 13, the solution with 6,000 mg/L initial fluoride concentration

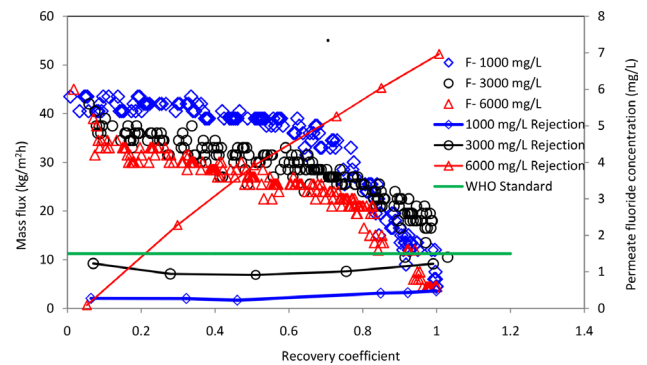


Fig. 13. Flux decline and wetting rate of different initial fluoride concentration (feed side/permeate side temperature = 60°C/20°C; feed/permeate volumetric flow rate = 1 L/min/1 L/min; membrane type = PTFE; humic acid = 30 mg/L; feed water = sample 3).

cannot even provide sufficient permeate water quality as the fluoride ion concentration in the permeate water surpasses the WHO maximum contaminant level (1.5 mg/L). Therefore, an optimum initial fluoride ion concentration for this specific type of feed water composition, operating characteristic, and membrane behavior will be a value close to or a little bit bigger than 3,000 mg/L. This can also be used as a methodology to set up an optimum initial fluoride ion concentration in treating highly polluted industrial wastewater using the DCMD process.

#### 4.3.2. Effect of membrane material and pore size

The experimental result attained for different pore sizes and membrane materials but under same operating conditions is quite interesting. As seen in Fig. 6, the experimental mass flux recorded for the 0.22  $\mu$ m PVDF membrane, 18.2 to 23.9 kg/m<sup>2</sup> h, is similar to that of the 0.45  $\mu$ m PVDF membrane, 22.5–29.5 kg/m<sup>2</sup> h. This shows that increasing the pore size of the membrane by more than two times (>100%) increased the flux over 19% which asserts a positive and direct correlation between membrane pore size and permeate flux. This flux increment is mainly attributed to the change induced in the mass transport mechanism resulted from the change of membrane pore size with respect to the mean free path of transported molecules. However, it is worth noting that increasing pore size enhances the permeate flux as a cost of distillate water quality deterioration because the contribution of viscous (Poiseuille) flow increases with increasing the pore size, which also enhances the diffusion of fluoride ion to the distillate side.

The study of the effect of using different membrane materials also underscores the considerable effect on the flux. Fig. 6 indicates an experiment conducted on pure water with only 20 mg/L fluoride and the result shows that the PTFE membrane yields a mass flux value of 36.5–42.9 kg/m<sup>2</sup> h, nearly twice the flux of the PVDF membrane (18.2–23.9 kg/m<sup>2</sup> h) of the same pore size (0.22  $\mu$ m). Moreover, an experiment conducted using highly fluoridated (1,000 mg/L fluoride) actual industrial wastewater (sample 3 of Table 4) has also revealed similar result in that the PTFE membrane provide better flux than the PVDF (Fig. 14). The increase in trans-membrane flux is likely attributed to the change of the mass transport mechanism from

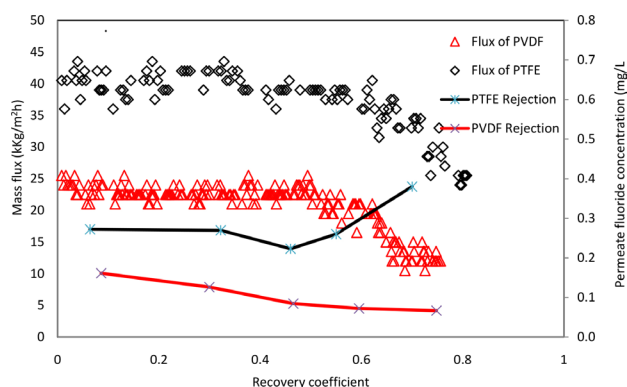


Fig. 14. Flux decline and wetting rate of different membrane materials (feed side/permeate side temperature = 60°C/20°C; feed/permeate volumetric flow rate = 1 L/min/1 L/min; membrane type = PTFE, fluoride concentration = 1,000 mg/L; humic acid = 30 mg/L; feed water = sample 3).

Knudsen diffusion to Knudsen-viscous transition [15]. More detailed reasons have been discussed in section 4.1. Hence the membrane material type and manufacturing method also affect the permeate flux in the DCMD process.

The effect of using different membrane material on fluoride rejection efficiency (wetting rate) has also been analyzed. All the graphical results (Figs. 11–13) synthesized either using the ultrapure water or the actual industrial wastewater shows that the PTFE membrane is better in providing higher flux, but PVDF is better in providing low fluoride distillate. The wetting rate in the PVDF membrane is also found to be much lower than that of PTFE. This substantial difference in distillate water quality is also attributable to the difference in their mass transport mechanism, overall material properties, and manufacturing methodologies of the two membranes. The contribution of Poiseuille flow is higher in PTFE membrane which favors the transport of fluoride ion to the permeate side.

#### 4.3.3. Effect of feed composition

For simplicity and to separately understand the contribution of each constituent of feed wastewater on the wetting behavior of the membrane, different combination of highly fluoridated feed water matrix (1,000 mg/L F<sup>-</sup>) has been considered. These include inorganic matters with high fluoride, organic matter with high fluoride, and both organic and inorganic matter with high fluoride. The detail ionic composition of the three wastewater samples has been tabulated in Table 4.

The experimental result drawn against the volume concentration factor (VCF) in Fig. 15 (black circle dots) using the inorganic wastewater (sample 1) shows that the permeate flux starts with a constant value of 39 kg/m<sup>2</sup>/h and stays until 15% recovery as there is no fouling. After this point, the feed solution starts to get saturated and nucleation and crystal growth start so that the flux drastically declines until 40% recovery. The saturation index value calculated using visual MINTEQ 3.1 with its corresponding speciation is indicated in Fig. 16. A positive value designates higher tendency of salt precipitation and membrane fouling which induce continuous flux declination from the concentration polarization effect of the inorganic substances that form thick and loose

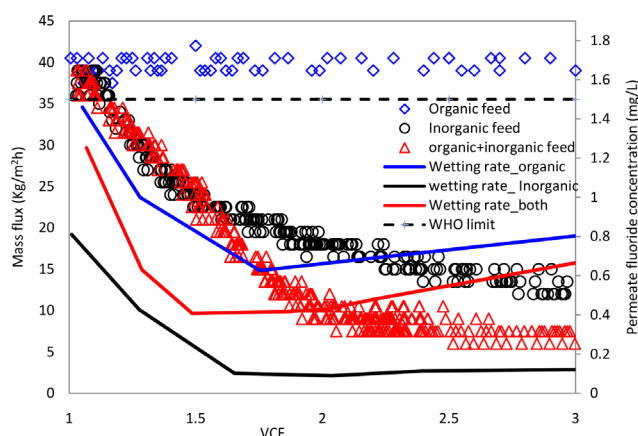


Fig. 15. Flux decline and wetting rate of different feed water composition (feed side/permeate side temperature = 60°C/20°C; feed/permeate volumetric flow rate = 1 L/min/1 L/min; membrane type = PTFE, fluoride concentration = 1,000 mg/L; humic acid = 30 mg/L).

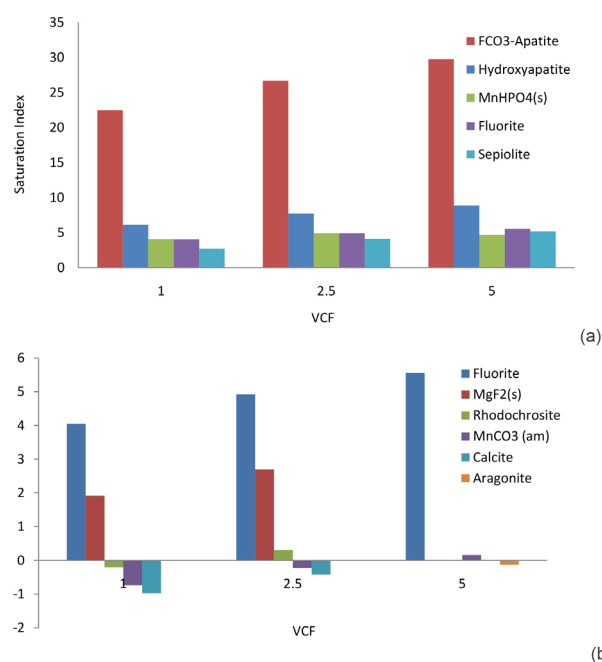


Fig. 16. Saturation index of wastewater sample 3 vs. VCF (a) sample with silicate and phosphate ions; (b) sample without phosphate and silicate ions.

whitish layer of inorganic bigger salt crystals covering the permeable membrane (Fig. 17). After 40% recovery point, the flux again tends to decline very slowly with an average value nearly 15 kg/m<sup>2</sup>/h which shows that fouling and cake layer formation reached its maximum value and build up of further layer is too slow but some vapor molecules can still be transported through the cake layer so that there is some amount of permeate yield. As to the rejection/wetting rate (the black line on Fig. 15), there is of three phase: first, there is high fluoride passage due to partial wetting, and then starts to suddenly decline due to the dilution effect and then stay constant for a while and increase back again due to the

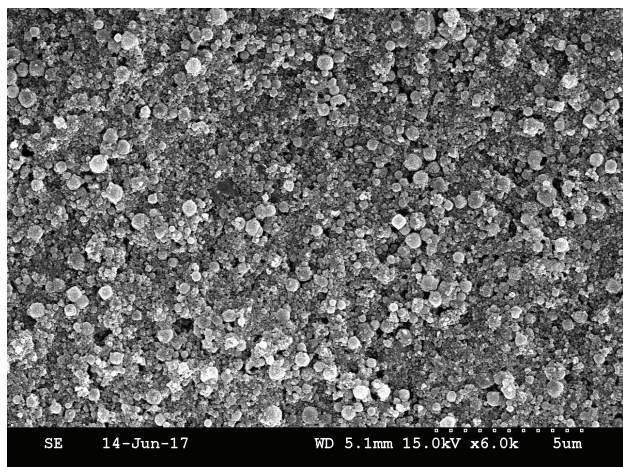


Fig. 17. SEM image of fouled membrane with inorganic salt crystals from apatite and fluorite materials (membrane type = PTFE, fluoride concentration = 1,000 mg/L, feed water = sample 1).

bridging effect created as a result of fouling. As indicated in the speciation analysis (Fig. 16) and the SEM image (Fig. 17), these inorganic foulants on the membrane surface are predominantly calcium fluoride as well as apatite and fluorite salts.

For highly fluoridated water sample (sample 2) consisting only organic matter (humic acid 30 mg/L), the permeate flux is quite steady (see blue diamond dots on Fig. 15) and stays almost constant with an average permeate flux value of 39 kg/m<sup>2</sup>/h over the experiment time. This is because, the deposition, in this case, is a thin layer and probably porous in its nature so that it supports passage of sufficient water vapor through both fouling layer and membrane body. However, the rejection/wetting rate (blue line on Fig. 15) follows the same trend as the inorganic except that wetting rate is significantly bigger in the organic fouling case. Therefore, the availability of organic substances in the wastewater sample takes the lion share responsibility toward the permeate quality reduction. A similar result has been indicated in a study conducted by Plattner et al. [12]. This higher wetting rate is induced because of brownish deposition and adsorption of organic matter on the membrane body which is mostly humic substance with a little bit inorganic salts of sodium (Fig. 18). It is quite often stated that organic matter highly affects the hydrophobicity of the membrane due to adsorption to the membrane surface [50,57] and by reducing LEP [18]. In order to verify this graphical result, the hydrophobicity loss of the membrane has also been measured as a function of loss of contact angle. Accordingly, the membrane with organic fouling exhibits the biggest contact angle loss. The contact angle value for the virgin, organic, inorganic, and mix of both, respectively, is 143° ± 3.2°, 70° ± 3.8°, 90.5° ± 4.1°, and 82.28° ± 3.2°.

The experiment carried out to study flux reduction (see Fig. 15) on a complex matrix comprising both organic and inorganic substances with high fluoride ion concentration (wastewater sample 3) shows that the permeate flux starts with an average constant value of 39 kg/m<sup>2</sup>/h and stays until 9% recovery as there is no fouling (see red triangles). From this point up to 50% recovery the flux tends to continuously

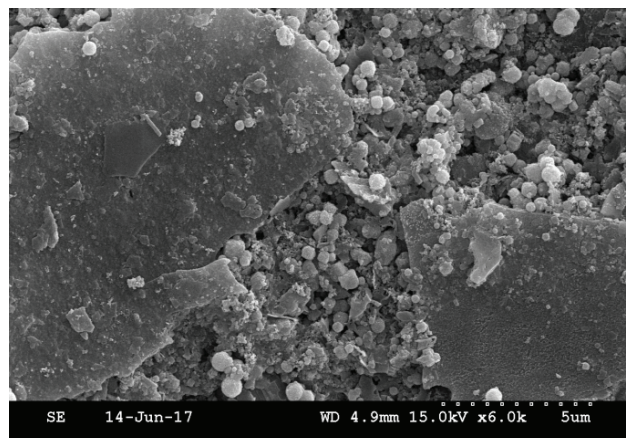


Fig. 18. SEM image of cake layer of organic fouling mixed with sodium salts (membrane type = PTFE, fluoride concentration = 1,000 mg/L; humic acid = 30 mg/L; feed water = sample 2).

drop until 9.2 kg/m<sup>2</sup>/h and stays almost constant thereafter. The sharp and steepest flux reduction trend, in this case, is more severe but closer in magnitude to the inorganic composition which asserts that the inorganic material takes the lion share responsibility for the major flux decline. However, the severity of flux decline and earlier fouling mainly appear from the early crystallization and agglomerative effect of organic matter when it comes in contact with the inorganic salts. This mixture of inorganic scales and organic foulant (Fig. 19) is relatively thicker, dense, and nonporous, and has quite different structure and composition resulted from the interactions between organic and inorganic foulant that favor humic acid and calcium fluoride to stick together. The relative fouling thickness is analyzed from the EDX image by looking at the amount of elements accumulated on the membrane surface. This thick layer is formed because organic materials reduce electrostatic repulsion and promote easy attachment of foulant on the membrane. The existence of this thick layer indicates the fact that organic materials play an important role in holding more deposit on the membrane surface through bindings of salt ions with functional groups of organic foulant [58].

As to the wetting rate, very interestingly, when both organic and inorganic substances are mixed, the fluoride rejection rate is quite significantly different from the expectation that when the influence of organic and inorganic is superimposed, the fluoride rejection rate supposed to decrease in the same manner as the flux. However, the aggregated effect of this mix solution on fluoride rejection rate is even found to be improved and exhibits an increasing trend. This is most likely because the thick layer of foulant on the membrane surface has created an impermeable media toward resisting mass transport of molecules. In spite of its small ionic size, fluoride ion has high charge density, and it is a more strongly hydrated ion and can have a bigger hydrated radius (nearly 0.36 nm) hence it might have bigger chance to be retained by this complex thick fouling layer through either steric effect or other exclusion mechanisms [59]. This experiment is continuously repeated to confirm the result and another solution of lighter concentration of organic (10 mg/L humic acid + 1,000 mg/L fluoride) has been considered and the result (Fig. 20) indicated that the fluoride

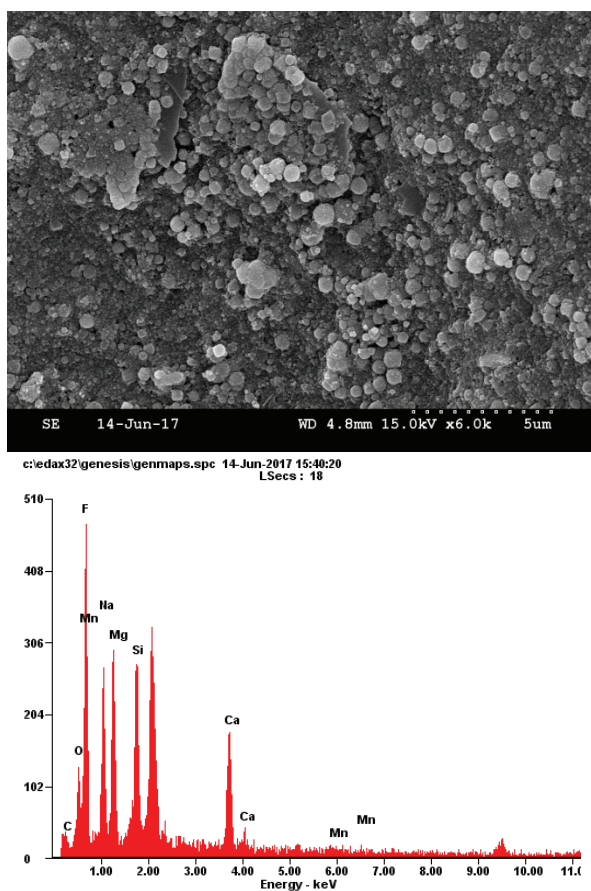


Fig. 19. SEM-EDX image of organic–inorganic mix thick and dense layer fouling showing higher accumulation of different elements including fluoride (membrane type = PTFE, fluoride concentration = 1,000 mg/L; humic acid = 30 mg/L; feed water = sample 3).

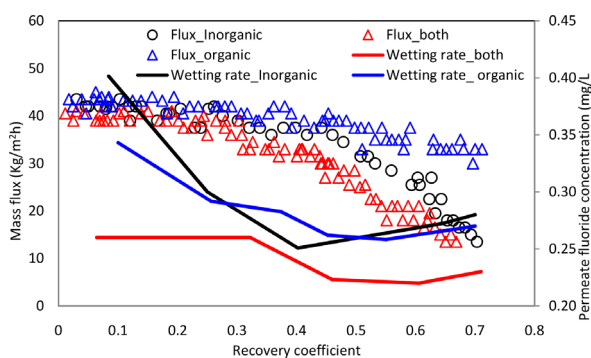


Fig. 20. Flux decline and wetting rate of different feed water composition (feed side/permeate side temperature = 60°C/20°C; feed/permeate volumetric flow rate = 1 L/min/1 L/min; membrane type = PTFE, fluoride concentration = 1,000 mg/L; humic acid = 15 mg/L; feed water = sample 2 diluted in 1 L/L).

rejection rate of mixture of both organic and inorganic is better than when they are treated separately. The contact angle of virgin and used membrane has also been measured to see the loss of hydrophobicity and to confirm the results in the figure. Subsequently, the measured value of the virgin membrane fouled with organic, inorganic, and a mix of both,

respectively, gives  $143^\circ \pm 3.2^\circ$ ,  $121.2^\circ \pm 3.1^\circ$ ,  $94.03^\circ \pm 5^\circ$ , and  $104.5^\circ \pm 4.2^\circ$ . This value also confirms that the wetting rate measured using contact angle also support there is a better performance of the membrane when both organic and inorganic foulant are mixed.

#### 4.3.4. Wetting control and regeneration mechanism

Chemical cleaning is the most common regeneration method for severely fouled membranes. Different chemical cleaning experiments using high pH, low pH, and chelating agents were tried alone or in combination (Table 5). Accordingly, organic fouling is found to be best cleaned by high pH solutions because humic acid organics are better decomposed and actively react at basic state. And inorganic substances are best cleaned by low pH because they react with the foulant's salt precipitates at lower pH. However, the fouling induced from combined organic and inorganic matters is found to be relatively difficult to remove neither by high pH nor by low pH. Therefore, low pH cleaning followed by high pH has been tried to achieve nearly 90% recovery. Lack of 100% flux recovery, in this case, might have been caused from an accumulation of some particles inside the membrane pores.

Even though excellent flux recovery can be achieved through chemical cleanings, post-cleaning-experiment has shown weaker fluoride rejection efficiency. This continuous increase in wetting rate is attributed to the interaction between the cleaning chemicals with the functional groups of the membranes, which finally leads to the irreversible hydrophobicity. Moreover, some particles from the fouling layer might have also deposited inside the pores of the membrane where cleaning chemicals may not reach. So that these stored particles favor transport of fluoride ion due to the bridging effect. The wetting rate of the membrane with the organic foulant has shown the fastest increase after the chemical cleaning.

## 5. Conclusions

The removal of fluoride ion from wastewater samples can be carried out effectively by using the DCMD process. A dusty gas model can be applied to model the entire mass transport mechanism through the hydrophobic PTFE and PVDF membranes. Factors such as feed water composition, operating characteristic, and membrane behavior have been identified as a controlling mechanism of the permeate flux magnitude and fluoride removal efficiency. Some of the major findings include:

- From the mass transfer analysis, the combined Knudsen–molecular–Poiseuille transition diffusion and combined Knudsen–Poiseuille diffusion are the dominant mass transfer mechanisms across 0.22  $\mu\text{m}$  flat sheet PVDF and PTFE membranes, respectively.
- Temperature variation significantly affects the mass transfer because of its exponential correlation with the vapor pressure. At higher temperatures, the lowest TPC and higher TE can be achieved. The flow rate, especially in the lower operating temperature range, has a small effect on increasing the flux.

Table 5  
Membrane cleaning experiment for organic, inorganic, and combined organic–inorganic

Type of wastewater sample	Cleaning agent utilized	Cleaning time	Flux recovery rate
Sample 1: Organic with high fluoride	Deionized water pH = 6.65	2 h	77%
	Low pH cleaning (pH = 2.5) using 0.5% (w) HCl	40 min	77%
	High pH cleaning (pH = 11.5) using 0.1% (w) NaOH	40 min	100%
	High pH cleaning 0.1% (w) NaOH and 0.03% (w) SDS (sodium dodecyl sulfate)	12 h	100%
Sample 2: Inorganic with high fluoride	Deionized water pH = 6.65	2 h	77%
	Low pH cleaning (pH = 2.5) using 0.5% (w) HCl	2 h	100%
	Low pH cleaning (pH = 3.5) using 2% (w) citric acid (C <sub>6</sub> H <sub>8</sub> O <sub>7</sub> )	2 h	100%
	Low pH cleaning (pH = 1.72) using formic acid	2 h	96%
	High pH solution (pH = 10) of 2% (w) of STPP (sodium tripolyphosphate, Na <sub>5</sub> P <sub>3</sub> O <sub>10</sub> ) and 0.8% (w) Na-EDTA sodium salt of ethylenediaminetetraacetic acid	10 h	92%
Sample 3: Both organic and inorganic with high fluoride	High pH cleaning (pH = 11.5) using 0.1% (w) NaOH	2 h	61%
	Low pH cleaning (pH = 3.5) using 2% (w) citric acid (C <sub>6</sub> H <sub>8</sub> O <sub>7</sub> )	2 h	77%
	High and low pH solutions combination: low pH cleaning using 2% (w) citric acid (C <sub>6</sub> H <sub>8</sub> O <sub>7</sub> ) (pH = 3.5) followed by high pH cleaning (pH = 11.5) using 0.1% (w) NaOH	2 h/1 h	96%

Note: % (w) or w/w refers to weight percentage of the cleaning chemical from the entire solvent weight.

- The DCMD process can effectively remove highly fluoridated water. However, depending on the target quality of permeate water, there is still a limit above which DCMD may not be capable enough to treat. With the methodology stated in this work, we can easily setup and identify an optimum initial fluoride ion concentration fitting certain feed water composition, membrane characteristic, and operating behavior.
- Increasing pore size enhances the permeate flux but it also reduces the distillate water quality. Due to the dominance of viscous and Knudsen type transport mechanism, PTFE membrane yields a mass flux value far better than the PVDF membrane but the PVDF membrane has a higher rejection efficiency and lower wetting rate.
- Depending on their concentration ratio, organic substances in the wastewater takes the biggest responsibility toward the permeate quality reduction and inorganic takes the biggest responsibility of the flux reduction. However, the aggregated effect of both is more severe in reducing the permeate flux but superior in improving the fluoride rejection rate. The fouled membrane recovered fully using chemical cleaning.
- DCMD is a technically feasible technology for defluoridation, as long as the membrane type, operating parameters and feed water behavior is carefully considered. This technology can also be an alternative option to be applied to remote, decentralized rural areas in developing countries that have sustainable renewable energy sources and high fluoride contents in their drinking water source. Developed countries with a substantial amount of fluoride in their industrial wastewater can also use the potential industrial waste energy for the economical application.

#### Acknowledgments

This research was supported by University of Science & Technology (Daejeon) and a grant (code 16IFIP-B065893-04) from the Industrial Facilities & Infrastructure Research Program funded by the Ministry of Land, Infrastructure, and Transport of the Korean government under the administration of the Korean Institute of Civil Engineering and Building Technology (KICT).

#### Symbols

$J_w$	—	Water vapor permeate flux, kg/m <sup>2</sup> h
$B_m$	—	DCMD coefficient of the membrane (membrane permeability), kg/m <sup>2</sup> s Pa
$P_{mf}^V$	—	Vapor pressure at the feed side of the membrane surface, Pa
$P_{mp}^V$	—	Vapor pressure at the permeate side of the membrane surface, Pa
$P_f^0$	—	Pure water partial vapor pressure at the feed side of the membrane surface, Pa
$\gamma_{wf}$	—	Water activity coefficient in the feed side
$\chi_{wf}$	—	Mole fraction/percent of water
$P_p^0$	—	Pure water partial vapor pressure at the permeate side of the membrane surface, Pa
$\chi_s$	—	Mole fraction/percent of solute
$T$	—	Membrane surface temperature feed side/permeate side, K
$T_m$	—	Average membrane temperature, K
$d_p$	—	Membrane pore diameter
$K_n$	—	Mass transfer mechanism constant, Knudsen number
$\lambda$	—	Mean free path of transported molecules

$K_B$	—	Boltzmann constant, J/K = $m^2 \cdot kg / (s^2 \cdot K)$
$P^a$	—	Total pressure inside the pore, Pa
$\delta_w^a$	—	Collision diameter for water vapor, m
$\delta_a^a$	—	Collision diameter for air, m
$M_w$	—	Molecular weights of water, kg/mol
$M_a$	—	Molecular weights of air, kg/mol
$PD_w$	—	Water air diffusion, Pa $m^2/s$
$\tau$	—	Membrane tortuosity
$\delta$	—	Membrane thickness, m
$K_{wf}$	—	Thermal conductivity of feed water in the feed side, W/m K
$K_{wp}$	—	Thermal conductivity of feed water in the permeate side, W/m K
$\Delta H_v$	—	Latent heat of vaporization, KJ/kg
$K_m$	—	Effective thermal conductivity of porous PTFE membrane, W/m K
$T_{mp}$	—	Membrane surface temperature on permeate side, K
$T_{mf}$	—	Membrane surface temperature on feed side, K
$h_f$	—	Feed side boundary layer heat transfer coefficient, W/m <sup>2</sup> K
$h_p$	—	Permeate side boundary layer heat transfer coefficient, W/m <sup>2</sup> K
$Nu_f$	—	Nusselt number of the feed side
$Nu_p$	—	Nusselt number of the permeate side
$D_h$	—	Flow channel hydraulic diameter, m
$A_c$	—	Cross-sectional area of the flow channel, m <sup>2</sup>
$P_w$	—	Wetted perimeter, m
$\text{Å}$	—	Angstroms = 100 picometer
$\mu$	—	Dynamic viscosity, kg/m s
$C_p$	—	Specific heat, J/kg K
$B_m^m$	—	Molecular diffusion based permeability coefficient, kg/m <sup>2</sup> s Pa
$B_m^k$	—	Knudsen diffusion based permeability coefficient, kg/m <sup>2</sup> s Pa
$B_m^c$	—	Combined Knudsen–molecular diffusion based permeability coefficient, kg/m <sup>2</sup> s Pa
$\tau$	—	Tortuosity
$\delta$	—	Thickness, m
$\epsilon$	—	Porosity
$r$	—	Pore diameter, m
$\Delta m$	—	Mass flux recorded per unit time, kg
$A_m$	—	Effective utilized area of the membrane
DCMD	—	Direct contact membrane distillation
MD	—	Membrane distillation
WHO	—	World Health Organization
TPC	—	Temperature polarization coefficient
TE	—	Thermal efficiency
PTFE	—	Polytetrafluoroethylene
PVDF	—	Polyvinylidene fluoride
VCF	—	Volume concentration factor
RO	—	Reverse osmosis
$R$	—	Gas constant, J/mol K
$\eta$	—	Viscosity of vapor air mixture, Pa s

## References

- [1] UNICEF, A Future Global Agenda For Children: The Links with Sanitation, Hygiene, Water and Environment, WaterFront, 12 (1999) 11–13.
- [2] WHO, Guidelines for Drinking-Water Quality: First Addendum to the Third Edition, Volume 1: Recommendations, WHO, Geneva, 2006, pp. 375–377.
- [3] Meenakshi, R.C. Maheshwari, Fluoride in drinking water and its removal, J. Hazard. Mater., 137 (2006) 456–463.
- [4] A. Heikens, S. Sumarti, M. van Bergen, B. Widianarko, L. Fokkert, K. van Leeuwe, W. Seinen, The impact of the hyperacid Ijen Crater Lake: risks of excess fluoride to human health, Sci. Total Environ., 346 (2005) 56–69.
- [5] D.L. Ozsvath, Fluoride and environmental health: a review, Rev. Environ. Sci. Biotechnol., 8 (2009) 59–79.
- [6] A.L. Choi, G. Sun, Y. Zhang, P. Grandjean, Developmental fluoride neurotoxicity: a systematic review and meta-analysis, Environ. Health Perspect., 120 (2012) 1362–1368.
- [7] A. Bhatnagar, E. Kumar, M. Sillanpää, Fluoride removal from water by adsorption—a review, Chem. Eng. J., 171 (2011) 811–840.
- [8] S.V. Jadhav, E. Bringas, G.D. Yadav, V.K. Rathod, I. Ortiz, K.V. Marathe, Arsenic and fluoride contaminated groundwaters: a review of current technologies for contaminants removal, J. Environ. Manage., 162 (2015) 306–325.
- [9] M. Mohapatra, S. Anand, B.K. Mishra, D.E. Giles, P. Singh, Review of fluoride removal from drinking water, J. Environ. Manage., 91 (2009) 67–77.
- [10] V. Tomar, D. Kumar, A critical study on efficiency of different materials for fluoride removal from aqueous media, Chem. Cent. J., 7 (2013) 1.
- [11] S. Chakraborty, M. Roy, P. Pal, Removal of fluoride from contaminated groundwater by cross flow nanofiltration: transport modeling and economic evaluation, Desalination, 313 (2013) 115–124.
- [12] J. Plattner, G. Naidu, T. Wintgens, S. Vigneswaran, C. Kazner, Fluoride removal from groundwater using direct contact membrane distillation (DCMD) and vacuum enhanced DCMD (VEDCMD), Sep. Purif. Technol., 180 (2017) 125–132.
- [13] M. BenSik Ali, B. Hamrouni, M. Dhahbi, Electrolytic defluorination of brackish water: effect of process parameters and water characteristics, Clean Soil Air Water, 38 (2010) 623–629.
- [14] Y.Z. Tan, J.W. Chew, W.B. Krantz, Effect of humic-acid fouling on membrane distillation, J. Membr. Sci., 504 (2016) 263–273.
- [15] M.S. El-Bourawi, Z. Ding, R. Ma, M. Khayet, A framework for better understanding membrane distillation separation process, J. Membr. Sci., 285 (2006) 4–29.
- [16] M. Khayet, T. Matsuura, Membrane Distillation: Principles and Applications, Elsevier, Oxford, UK, 2011.
- [17] L.M. Camacho, L. Dumée, J. Zhang, J. Li, M. Duke, J. Gomez, S. Gray, Advances in membrane distillation for water desalination and purification applications, Water, 5 (2013) 94–196.
- [18] A. Alkhdhiri, N. Darwish, N. Hilal, Membrane distillation: a comprehensive review, Desalination, 287 (2012) 2–18.
- [19] A.M. Alkhaib, N. Lior, Membrane-distillation desalination: status and potential, Desalination, 171 (2005) 111–131.
- [20] G. Naidu, S. Jeong, S. Vigneswaran, T.-M. Hwang, Y.-J. Choi, S.-H. Kim, A review on fouling of membrane distillation, Desal. Wat. Treat., 57 (2016) 10052–10076.
- [21] L. Feenstra, L. Vasak, J. Griffioen, IGRAC-SP2007-1 Fluoride-removal, International Groundwater Resources Assessment Centre, DELFT, The Netherlands, 2007.
- [22] A. Boubakri, R. Bouchrit, A. Hafiane, S.A.-T. Bouguecha, Fluoride removal from aqueous solution by direct contact membrane distillation: theoretical and experimental studies, Environ. Sci. Pollut. Res., 21 (2014) 10493–10501.
- [23] D. Hou, J. Wang, C. Zhao, B. Wang, Z. Luan, X. Sun, Fluoride removal from brackish groundwater by direct contact membrane distillation, J. Environ. Sci., 22 (2010) 1860–1867.
- [24] S. Yarlagadda, V.G. Gude, L.M. Camacho, S. Pinappu, S. Deng, Potable water recovery from As, U, and F contaminated ground waters by direct contact membrane distillation process, J. Hazard. Mater., 192 (2011) 1388–1394.
- [25] D. Hou, J. Wang, X. Sun, Z. Luan, C. Zhao, X. Ren, Boron removal from aqueous solution by direct contact membrane distillation, J. Hazard. Mater., 177 (2010) 613–619.

- [26] A. Boubakri, S.A.-T. Bouguecha, I. Dhaouadi, A. Hafiane, Effect of operating parameters on boron removal from seawater using membrane distillation process, *Desalination*, 373 (2015) 86–93.
- [27] A.K. Manna, M. Sen, A.R. Martin, P. Pal, Removal of arsenic from contaminated groundwater by solar-driven membrane distillation, *Environ. Pollut.*, 158 (2010) 805–811.
- [28] D. Qu, J. Wang, D. Hou, Z. Luan, B. Fan, C. Zhao, Experimental study of arsenic removal by direct contact membrane distillation, *J. Hazard. Mater.*, 163 (2009) 874–879.
- [29] A. Boubakri, A. Hafiane, S. Al Tahar Bouguecha, Nitrate removal from aqueous solution by direct contact membrane distillation using two different commercial membranes, *Desal. Wat. Treat.*, 56 (2015) 2723–2730.
- [30] M. Bhattacharya, S.K. Dutta, J. Sikder, M.K. Mandal, Computational and experimental study of chromium (VI) removal in direct contact membrane distillation, *J. Membr. Sci.*, 450 (2014) 447–456.
- [31] D. Qu, D. Sun, H. Wang, Y. Yun, Experimental study of ammonia removal from water by modified direct contact membrane distillation, *Desalination*, 326 (2013) 135–140.
- [32] Ó. Andrésdóttir, C. Ong, M. Nabavi, S. Paredes, A. Khalil, B. Michel, D. Poulikakos, An experimentally optimized model for heat and mass transfer in direct contact membrane distillation, *Int. J. Heat Mass Transfer*, 66 (2013) 855–867.
- [33] M. Qtaishat, T. Matsuura, B. Kruczek, M. Khayet, Heat and mass transfer analysis in direct contact membrane distillation, *Desalination*, 219 (2008) 272–292.
- [34] F. Laganà, G. Barbieri, E. Drioli, Direct contact membrane distillation: modelling and concentration experiments, *J. Membr. Sci.*, 166 (2000) 1–11.
- [35] Y.M. Manawi, M. Khraisheh, A.K. Fard, F. Benyahia, S. Adham, Effect of operational parameters on distillate flux in direct contact membrane distillation (DCMD): comparison between experimental and model predicted performance, *Desalination*, 336 (2014) 110–120.
- [36] J. Phattaranawik, R. Jiraratananon, A.G. Fane, Heat transport and membrane distillation coefficients in direct contact membrane distillation, *J. Membr. Sci.*, 212 (2003) 177–193.
- [37] A. Hausmann, P. Sanciolo, T. Vasiljevic, U. Kulozik, M. Duke, Performance assessment of membrane distillation for skim milk and whey processing, *J. Dairy Sci.*, 97 (2014) 56–71.
- [38] S. Srisurichan, R. Jiraratananon, A.G. Fane, Mass transfer mechanisms and transport resistances in direct contact membrane distillation process, *J. Membr. Sci.*, 277 (2006) 186–194.
- [39] M.A. Izquierdo-Gil, C. Fernández-Pineda, M.G. Lorenz, Flow rate influence on direct contact membrane distillation experiments: different empirical correlations for Nusselt number, *J. Membr. Sci.*, 321 (2008) 356–363.
- [40] P. Moghaddam Kamrani, O. Bakhtiari, P. Kazemi, T. Mohammadi, Theoretical modeling of direct contact membrane distillation (DCMD): effects of operation parameters on flux, *Desal. Wat. Treat.*, 56 (2015) 2013–2022.
- [41] Z. Ding, R. Ma, A.G. Fane, A new model for mass transfer in direct contact membrane distillation, *Desalination*, 151 (2003) 217–227.
- [42] A. Ali, F. Macedonio, E. Drioli, S. Aljlil, O.A. Alharbi, Experimental and theoretical evaluation of temperature polarization phenomenon in direct contact membrane distillation, *Chem. Eng. Res. Des.*, 91 (2013) 1966–1977.
- [43] Y. Guan, J. Li, F. Cheng, J. Zhao, X. Wang, Influence of salt concentration on DCMD performance for treatment of highly concentrated NaCl, KCl, MgCl<sub>2</sub> and MgSO<sub>4</sub> solutions, *Desalination*, 355 (2015) 110–117.
- [44] L. Martínez, Comparison of membrane distillation performance using different feeds, *Desalination*, 168 (2004) 359–365.
- [45] T.Y. Cath, V.D. Adams, A.E. Childress, Experimental study of desalination using direct contact membrane distillation: a new approach to flux enhancement, *J. Membr. Sci.*, 228 (2004) 5–16.
- [46] S.T. Hsu, K.T. Cheng, J.S. Chiou, Seawater desalination by direct contact membrane distillation, *Desalination*, 143 (2002) 279–287.
- [47] J.P. Holman, *Heat Transfer*, 10th ed., McGraw Hill Higher Education, Boston, 2010.
- [48] E. Guillen-Burrieza, M.O. Mavukkandy, M.R. Bilad, H.A. Arafat, Understanding wetting phenomena in membrane distillation and how operational parameters can affect it, *J. Membr. Sci.*, 515 (2016) 163–174.
- [49] G. Naidu, S. Jeong, S.-J. Kim, I.S. Kim, S. Vigneswaran, Organic fouling behavior in direct contact membrane distillation, *Desalination*, 347 (2014) 230–239.
- [50] S. Srisurichan, R. Jiraratananon, A.G. Fane, Humic acid fouling in the membrane distillation process, *Desalination*, 174 (2005) 63–72.
- [51] R. Huo, Z. Gu, K. Zuo, G. Zhao, Preparation and humic acid fouling resistance of poly(vinylidene fluoride)-fabric composite membranes for membrane distillation, *J. Appl. Polym. Sci.*, 117 (2010) 3651–3658.
- [52] T.-C. Chen, C.-D. Ho, H.-M. Yeh, Theoretical modeling and experimental analysis of direct contact membrane distillation, *J. Membr. Sci.*, 330 (2009) 279–287.
- [53] L. Martínez, F.J. Florido-Díaz, A. Hernández, P. Prádanos, Characterisation of three hydrophobic porous membranes used in membrane distillation, *J. Membr. Sci.*, 203 (2002) 15–27.
- [54] H.J. Hwang, K. He, S.R. Gray, J. Zhang, I.S. Moon, Direct contact membrane distillation (DCMD): experimental study on the commercial PTFE membrane and modelling, *J. Membr. Sci.*, 371 (2011) 90–98.
- [55] B.R. Min, A.L. Gill, W.N. Gill, A note on fluoride removal by reverse osmosis, *Desalination*, 49 (1984) 89–93.
- [56] P.I. Ndiaye, P. Moulin, L. Dominguez, J.C. Millet, F. Charbit, Removal of fluoride from electronic industrial effluent by RO membrane separation, *Desalination*, 173 (2005) 25–32.
- [57] S. Meng, Y. Ye, J. Mansouri, V. Chen, Fouling and crystallization behavior of superhydrophobic nano-composite PVDF membranes in direct contact membrane distillation, *J. Membr. Sci.*, 463 (2014) 102–112.
- [58] Q.-M. Nguyen, S. Jeong, S. Lee, Characteristics of membrane foulants at different degrees of SWRO brine concentration by membrane distillation, *Desalination*, 409 (2017) 7–20.
- [59] L.A. Richards, M. Vuachère, A.I. Schäfer, Impact of pH on the removal of fluoride, nitrate and boron by nanofiltration/reverse osmosis, *Desalination*, 261 (2010) 331–337.